New extended Skyrme interaction for nuclear properties and nuclear reactions

Yongli Xu,[1,*] Hairui Guo,[2] Yinlu Han,[3,†] and Qingbiao Shen[3]

[1]*College of Physics and Electronic Science, Shanxi Datong University, Datong 037009, China*
[2]*Institute of Applied Physics and Computational Mathematics, Beijing 100094, China*
[3]*Key Laboratory of Nuclear Data, China Institute of Atomic Energy, P. O. Box 275-41, Beijing 102413, China*

The extended Skyrme interaction involving additional momentum- and density-dependent terms is adopted to uniformly describe the properties of nuclear matter and finite nuclei, as well as the nuclear reaction properties. A new set of extended Skyrme interaction parameters is constructed by simultaneously fitting the properties of nuclear matter and the experimental data of finite nuclei and neutron-nucleus scattering observables. These data include the binding energies and charge rms radii of some spherical even-even nuclei, the total cross sections, nonelastic cross sections, elastic-scattering angular distributions, and analyzing powers. Compared with the existing Skyrme interactions, the obtained extended Skyrme interaction has a significantly improvement in the agreement with corresponding experimental data, together with some additional constraints on nuclear matter.

I. INTRODUCTION

The nucleon-nucleon interaction plays a key role in the study of nuclear properties. Generally, effective and realistic nucleon-nucleon interactions are used by different microscopic approaches. However, the realistic nucleon-nucleon interaction has still some challenges for microscopic many-body theory because of the limitations in the techniques for solving the nuclear many-body problem. For effective nucleon-nucleon interaction, it has been widely applied in many branches of nuclear physics and astrophysics since the nonrelativistic zero-range density and momentum-dependent Skyrme-type effective nucleon-nucleon interaction was proposed in 1950s [1]. In particular, the Skyrme interaction was applied in the study of finite nuclei in the Hartree-Fock (HF) model [2]. It greatly simplifies the calculations with the zero-range form and has been successfully used to describe binding energies, charge rms radii, and excited states of finite nuclei as well as the properties of nuclear matter around saturation density.

In the past few years, a lot of work had been devoted to constructing the Skyrme interactions of standard form to better reproduce the ground-state and spectroscopic properties of nuclei, especially of exotic ones, and the properties of excited states of nuclei [3–7]. It is of interest to extend the field of application of the Skyrme interactions to describe the nuclear scattering processes [8]. We also presented two sets of standard Skyrme interactions, SkC and SkD [9], by simultaneously fitting the properties of nuclear matter and finite nuclei, as well as the neutron-induced reaction cross sections and polarization data. The neutron-induced reactions on light and actinide nuclei below 100 MeV were predicted by the obtained Skyrme interaction SkC. Moreover, we also predicted the scattering observables in the target mass range $148 \leqslant A \leqslant 194$, which are superdeformed nuclei and have

rich nuclear structure properties [10]. All of the theoretical results give reasonable agreements with the corresponding experimental data.

The recent research results show that the conventional standard Skyrme interaction met challenges in the prediction of variously instable nuclear matter around saturation density or at supra-saturation densities, so it is necessary to extend the standard Skyrme interaction [11,12]. Compared with the standard Skyrme interaction, the extended Skyrme interaction involves additional density- and momentum-dependent terms to effectively simulate the momentum dependence of three-body force. Through the extended Skyrme interaction, the research has been devoted to describing the properties of the nuclear matter and the astrophysics problem, such as studying the properties of neutron stars [13–16]. Although these existing extended Skyrme interactions can well predict the properties of nuclear matter and reproduce the properties of finite nuclei, they cannot make a good description for the properties of nuclear reaction even if some experimental data for elastic-scattering angular distributions were considered in the parametrizations of the extended Skyrme force, such as SkOP family [17].

In this paper, a new set of extended Skyrme interaction parameters is constructed by simultaneously fitting the nuclear-matter saturation properties, the finite nuclei ground-state properties, and the neutron-nucleus scattering data below 100 MeV. The obtained extended Skyrme interaction can well describe not only the properties of nuclear matter and finite nuclei but also the properties of the nuclear reaction. Furthermore, the reactions of neutron-induced light, actinide, and deformed nuclei are predicted by the new extended Skyrme interaction.

The paper is organized as follows. In Sec. II, the theoretical model and methods adopted are shown. In Sec. III, the experimental data and constrains used in our fitting are described. Further, the new set of extended Skyrme interaction parameters are presented. The calculation results and some analysis are given in Sec. IV. Finally, the conclusion is summarized in Sec. V.

_____
*xuyongli776@126.com
†hanyl@ciae.ac.cn

II. THE THEORETICAL MODELS AND METHODS

The two-body effective interaction is generally described by the so-called standard Skyrme interaction (see, e.g., Refs. [9,18]):

$$
\begin{aligned}
V_{1,2}(\vec{R},\vec{r}) = {} & t_0(1 + x_0 P^\sigma)\delta(\vec{r}) + \tfrac{1}{2}t_1(1 + x_1 P^\sigma)[\vec{k'}^2\delta(\vec{r}) \\
& + \delta(\vec{r})\vec{k}^2] + t_2(1 + x_2 P^\sigma)\vec{k'}\cdot\delta(\vec{r})\vec{k} \\
& + \tfrac{1}{6}t_3(1 + x_3 P^\sigma)\rho^\alpha(\vec{R})\delta(\vec{r}) \\
& + iW_0(\vec{\sigma}_1 + \vec{\sigma}_2)\cdot[\vec{k'}\times\delta(\vec{r})\vec{k}],
\end{aligned} \tag{1}
$$

where $\vec{r} = \vec{r}_1 - \vec{r}_2$ and $\vec{R} = (\vec{r}_1 + \vec{r}_2)/2$ are the relative and center-of-mass radius vectors, $\vec{k} = -i(\vec{\nabla}_1 - \vec{\nabla}_2)/2$ acting on the right and its Hermitian conjugate operator $\vec{k'}$ acting on the left are respectively the operators of momentum of the nucleon relative motion in the initial and final states, P^σ is the spin exchange operator, and $\vec{\sigma}$ is the Pauli spin matrix.

In the present work, the extended Skyrme interaction is adopted to effectively account for the momentum dependence of the three-body interaction, which includes the following additional zero-range density- and momentum-dependent terms [7,14,15,19]:

$$
\begin{aligned}
& + \tfrac{1}{2}t_4(1 + x_4 P^\sigma)[\vec{k'}^2\rho^{\alpha_4}(\vec{R})\delta(\vec{r}) + \delta(\vec{r})\rho^{\alpha_4}(\vec{R})\vec{k}^2] \\
& + t_5(1 + x_5 P^\sigma)\vec{k'}\cdot\rho^{\alpha_5}(\vec{R})\delta(\vec{r})\vec{k}.
\end{aligned} \tag{2}
$$

Compared with the standard Skyrme interaction, the adjustable Skyrme parameters $t_4, t_5, x_4, x_5, \alpha_4, \alpha_5$ are added in the present extended Skyrme interaction.

A. The nucleon microscopic optical model potential with the extended Skyrme interaction

Just like the method used in Refs. [9,18], the nucleon microscopic optical potential (MOP) is achieved from the calculation of the mass operator of the one-particle Green's function by perturbation theory up to the Feynman diagrams of the second order. For simplicity, the nuclear-matter approximation is used in the calculation. In the nuclear matter, the nucleon wave function is taken as the plane-wave function.

Using the extended Skyrme interaction, the real part of nucleon MOP is expressed as

$$
\begin{aligned}
V_{\tau_\alpha} = {} & \frac{m^*_{\tau_\alpha}}{m_{\tau_\alpha}}\left\{g_0\rho - h_0\rho_{\tau_\alpha} + \frac{1}{4}\left[\left(g_1 + g_2 + \frac{1}{6}g_3\rho^\alpha\rho + g_4\rho^{\alpha_4} + g_5\rho^{\alpha_5}\right) - \left(h_1 - h_2 + \frac{1}{6}h_3\rho^\alpha + h_4\rho^{\alpha_4} - h_5\rho^{\alpha_5}\right)\rho_{\tau_\alpha}\right] \right. \\
& \times \frac{2m_{\tau_\alpha}}{\hbar^2}\left(\frac{M}{M + m_{\tau_\alpha}}E_L - V_C\right) + \frac{1}{20\pi^2}\left[(g_1 + g_2 + g_4\rho^{\alpha_4} + g_5\rho^{\alpha_5} - h_1 + h_2 - h_4\rho^{\alpha_4} + h_5\rho^{\alpha_5})k^5_{\tau_\alpha}\right. \\
& \left.\left. + (g_1 + g_2 + g_4\rho^{\alpha_4} + g_5\rho^{\alpha_5})k^5_{-\tau_\alpha}\right]\right\},
\end{aligned} \tag{3}
$$

where g_i and h_i are introduced notation for the extended Skyrme interaction parameter combinations and written as

$$
g_i = t_i\left(1 + \tfrac{1}{2}x_i\right), \quad h_i = t_i\left(\tfrac{1}{2} + x_i\right). \tag{4}
$$

k_{τ_α} is the Fermi momentum of the nucleon τ_α. E_L is the incident nucleon energy in the laboratory. m_{τ_α} and M are respectively the mass of nucleon and target, and the nucleon effective mass m^* is given by

$$
\frac{m^*_{\tau_\alpha}}{m_{\tau_\alpha}} = \left\{1 + \frac{m_{\tau_\alpha}}{2\hbar^2}\left[(g_1 + g_2 + g_4\rho^{\alpha_4} + g_5\rho^{\alpha_5})\rho - (h_1 - h_2 + h_4\rho^{\alpha_4} - h_5\rho^{\alpha_5})\rho_{\tau_\alpha}\right]\right\}^{-1}. \tag{5}
$$

The Coulomb potential in the nuclear matter V_C is taken as

$$
V_C = \frac{3zZe^2}{2R_C}. \tag{6}
$$

Obviously, the real part of nucleon MOP has a linear relation with E_L and is isospin dependent. The W_0 term in Skyrme interaction expression has no contribution to the real part of nucleon MOP.

Moreover, the imaginary part of nucleon MOP is expressed as

$$
W_A = -\frac{\pi}{(2\pi)^6}\sum_{i=1}^{7}W_i, \tag{7}
$$

where

$$
W_1 = \left(2g_{00} + \tfrac{2}{3}g_{03}\rho^\alpha + \tfrac{1}{18}g_{33}\rho^{2\alpha}\right)[I_1(\tau_\alpha,\tau_\alpha) + I_1(\tau_\alpha,-\tau_\alpha)] - \left(2h_{00} + \tfrac{2}{3}h_{03}\rho^\alpha + \tfrac{1}{18}h_{33}\rho^{2\alpha}\right)I_1(\tau_\alpha,\tau_\alpha), \tag{8}
$$

$$
W_2 = \left[g_{01} + g_{04}\rho^{\alpha_4} + \tfrac{1}{6}\rho^\alpha(g_{13} + g_{34}\rho^{\alpha_4})\right][I_2(\tau_\alpha,\tau_\alpha) + I_2(\tau_\alpha,-\tau_\alpha)] - \left[h_{01} + h_{04}\rho^{\alpha_4} + \tfrac{1}{6}\rho^\alpha(h_{13} + h_{34}\rho^{\alpha_4})\right]I_2(\tau_\alpha,\tau_\alpha), \tag{9}
$$

$$
W_3 = \tfrac{1}{8}(g_{11} + 2g_{14}\rho^{\alpha_4} + g_{44}\rho^{2\alpha_4})[I_3(\tau_\alpha,\tau_\alpha) + I_3(\tau_\alpha,-\tau_\alpha)] - \tfrac{1}{8}(h_{11} + 2h_{14}\rho^{\alpha_4} + h_{44}\rho^{2\alpha_4})I_3(\tau_\alpha,\tau_\alpha), \tag{10}
$$

$$
W_4 = \left[g_{02} + g_{05}\rho^{\alpha_5} + \tfrac{1}{6}\rho^\alpha(g_{23} + g_{35}\rho^{\alpha_5})\right]I_4(\tau_\alpha,-\tau_\alpha), \tag{11}
$$

$$W_5 = \tfrac{1}{4}(g_{12} + g_{24}\rho^{\alpha_4} + g_{15}\rho^{\alpha_5} + g_{45}\rho^{\alpha_4+\alpha_5})I_5(\tau_\alpha, -\tau_\alpha),$$ (12)

$$W_6 = \tfrac{1}{8}(g_{22} + 2g_{25}\rho^{\alpha_5} + g_{55}\rho^{2\alpha_5})[I_6(\tau_\alpha,\tau_\alpha) + I_6(\tau_\alpha,-\tau_\alpha)] - \tfrac{1}{8}(h_{22} + 2h_{25}\rho^{\alpha_5} + h_{55}\rho^{2\alpha_5})I_6(\tau_\alpha,\tau_\alpha),$$ (13)

$$W_7 = \tfrac{1}{4}W_0^2[2I_7(\tau_\alpha,\tau_\alpha) + I_7(\tau_\alpha,-\tau_\alpha)],$$ (14)

where the notation g_{ij} and h_{ij} are defined by

$$g_{ij} = t_i t_j\big[1 + x_i x_j + \tfrac{1}{2}(x_i + x_j)\big],$$ (15)

$$h_{ij} = t_i t_j\big[x_i + x_j + \tfrac{1}{2}(1 + x_i x_j)\big].$$ (16)

The quantities $I_i(\tau_\alpha,\tau_\nu)$ are integrals over the momenta of intermediate nucleon states, which arise in the calculations of the imaginary part of MOP from the second-order diagrams, and the detailed expressions are provided in Ref. [18].

For a finite nucleus MOP, the simplest way is to use the local density approximation (LDA) [20]. As in the previous works [18,21,22], the nuclear densities are expressed by the Negele's empirical formula.

B. Extended Skyrme-Hartree-Fock model

In the Skyrme-Hartree-Fock (SHF) approach, calculation of double closed-shell spherical nuclei with the extended Skyrme interaction, the central potential $U_\tau(r)$ of a nucleus can be expressed as

$$
\begin{aligned}
U_\tau(r) ={}& \rho g_0 - \rho_\tau h_0 + \frac{1}{4}(g_1 + g_2 + g_4\rho^{\alpha_4} + g_5\rho^{\alpha_5})T - \frac{1}{4}(h_1 - h_2 + h_4\rho^{\alpha_4} - h_5\rho^{\alpha_5})T_\tau + \frac{1}{6}\rho^\alpha(\rho g_3 - \rho_\tau h_3) \\
&+ \frac{\alpha}{12}\big[g_3\rho^{1+\alpha} - h_3(\rho_n^2 + \rho_p^2)\rho^{\alpha-1}\big] + \frac{1}{4}(\alpha_4 g_4\rho^{\alpha_4} + \alpha_5 g_5\rho^{\alpha_5})T - \frac{1}{4}(\alpha_4 h_4\rho^{\alpha_4-1} - \alpha_5 h_5\rho^{\alpha_5-1})(\rho_n T_n + \rho_p T_p) \\
&- \frac{1}{8}[3g_1 - g_2 + (3 + 2\alpha_4)g_4\rho^{\alpha_4} - g_5\rho^{\alpha_5}]\vec{\nabla}^2\rho + \frac{1}{8}[3h_1 + h_2 + 3h_4\rho^{\alpha_4} + h_5\rho^{\alpha_5}]\vec{\nabla}^2\rho_\tau \\
&- \frac{1}{16}[(3 + 2\alpha_4)\alpha_4 g_4\rho^{\alpha_4-1} - \alpha_5 g_5\rho^{\alpha_5-1}](\vec{\nabla}\rho)^2 + \frac{1}{8}\alpha_4 h_4\rho^{\alpha_4-1}(\rho_\tau\vec{\nabla}^2\rho + \rho_n\vec{\nabla}^2\rho_n + \rho_p\vec{\nabla}^2\rho_p) \\
&+ \frac{1}{8}(3\alpha_4 h_4\rho^{\alpha_4-1} + \alpha_5 h_5\rho^{\alpha_5-1})(\vec{\nabla}\rho\cdot\vec{\nabla}\rho_\tau) - \frac{1}{16}(\alpha_4 h_4\rho^{\alpha_4-1} + \alpha_5 h_5\rho^{\alpha_5-1})[(\vec{\nabla}\rho_n)^2 + (\vec{\nabla}\rho_p)^2] \\
&+ \frac{1}{8}\alpha_4(\alpha_4 - 1)h_4\rho^{\alpha_4-2}\rho_\tau(\vec{\nabla}\rho)^2 - \frac{1}{16}(\alpha_4 t_4 x_4\rho^{\alpha_4-1} + \alpha_5 t_5 x_5\rho^{\alpha_5-1})J^2 + \frac{1}{16}(J_n^2 + J_p^2)(\alpha_4 t_4\rho^{\alpha_4-1} - \alpha_5 t_5\rho^{\alpha_5-1}) \\
&- \frac{1}{2}W_0(\vec{\nabla}\cdot\vec{J} + \vec{\nabla}\cdot\vec{J}_\tau) + U_C(\vec{r})\delta_{\tau,-\frac{1}{2}},
\end{aligned}
$$ (17)

and the spin-orbit potential $U_\tau^{LS}(r)$ is written as

$$U_\tau^{LS}(r) = \frac{1}{2r}W_0\left(\frac{d\rho}{dr} + \frac{d\rho_\tau}{dr}\right) + \frac{1}{8r}[(t_1 - t_2 + t_4\rho^{\alpha_4} - t_5\rho^{\alpha_5})\vec{J}_\tau - (t_1 x_1 + t_2 x_2 + t_4 x_4\rho^{\alpha_4} + t_5 x_5\rho^{\alpha_5})\vec{J}],$$ (18)

where $\rho = \rho_n + \rho_p$, $T = T_n + T_p$, and $J = J_n + J_p$ are, respectively, the particle number density, kinetic energy density, and spin density, with p and n denoting the proton and neutron. The subscript τ refers to neutron ($\tau = \frac{1}{2}$) or proton ($\tau = -\frac{1}{2}$). The notations g_i and h_i are the same as in Eq. (3). The Coulomb potential $U_C(r)$ takes into account the direct and exchange parts and can be expressed as

$$U_C(r) = \int \rho_p(\vec{r}')\frac{e^2}{|\vec{r} - \vec{r}'|}d\vec{r}' - e^2\left(\frac{3}{\pi}\right)^{1/3}\rho_p^{1/3}(\vec{r}).$$ (19)

In addition, the eigenvalue in the HF equation is replaced with the continuous-variable energy and the wave function is also modified by introducing a transformation [9,23]. The real part of the spin-orbit potential considered the correlation with the incident nucleon energy, while the imaginary part of the spin-orbit potential below 100 MeV is usually omitted [9]. Meanwhile, we also take the real spin-orbit potential in the SHF theory of finite nuclei [Eq. (18)] as the spin-orbit part of MOP.

C. The properties of nuclear matter and the Landau parameters

The macroscopic quantities of symmetrical nuclear matter, including the energy per nucleon E/A, the incompressibility K, and the symmetry energy $E_{\rm sym}$ are respectively expressed with extended Skyrme interaction parameters as follows:

$$\frac{E}{A} = \frac{3}{5}\frac{\hbar^2}{2m}k_F^2 + \frac{1}{16}\rho(6t_0 + t_3\rho^\alpha) + \frac{3}{80}\rho k_F^2(3t_1 + 5t_2 + 4t_2x_2 + 3t_4\rho^{\alpha_4} + 5t_5\rho^{\alpha_5} + 4t_5x_5\rho^{\alpha_5}), \tag{20}$$

$$K = \frac{6}{5}\frac{\hbar^2}{2m}k_F^2 + \frac{3}{16}\rho[12t_0 + t_3\rho^\alpha(1+\alpha)(2+3\alpha)] + \frac{3}{80}\rho k_F^2[60t_1 + 300t_2 + 80t_2x_2 + 3t_4\rho^{\alpha_4}(4+3\alpha_4)(5+3\alpha_4)$$
$$+ 5t_5\rho^{\alpha_5}(4+3\alpha_5)(5+3\alpha_4) + 4t_5x_5\rho^{\alpha_5}(4+3\alpha_5)(5+3\alpha_4)], \tag{21}$$

$$E_{\rm sym} = \frac{1}{3}\frac{\hbar^2}{2m}k_F^2 - \frac{1}{8}\rho\left[t_0(1+2x_0) + \frac{1}{6}t_3\rho^\alpha(1+2x_3)\right] - \frac{1}{24}\rho k_F^2[3t_1x_1 - t_2(4+5x_2) + 3t_4x_4\rho^{\alpha_4} - t_5\rho^{\alpha_5}(4+5x_5)]. \tag{22}$$

The symmetry energy $E_{\rm sym}$ can be expanded around saturation density ρ_0 in terms of the density slope $L(\rho_0)$ as

$$E_{\rm sym}(\rho) = E_{\rm sym}(\rho_0) + \frac{L(\rho_0)}{3}\left(\frac{\rho - \rho_0}{\rho_0}\right) + o[(\rho - \rho_0)^2]. \tag{23}$$

Using the presented symmetry energy $E_{\rm sym}$ expression, the saturation density slope $L(\rho_0)$ is expressed as

$$L(\rho_0) = \frac{2}{3}\frac{\hbar^2}{2m}\left(\frac{3\pi^2}{2}\right)^{\frac{2}{3}}\rho_0^{\frac{2}{3}} - \frac{3}{8}t_0(1+2x_0)\rho_0 - \frac{5}{8}t_1x_1\left(\frac{3\pi^2}{2}\right)^{\frac{2}{3}}\rho_0^{\frac{5}{3}} + \frac{5}{24}t_2(4+5x_2)\left(\frac{3\pi^2}{2}\right)^{\frac{2}{3}}\rho_0^{\frac{5}{3}}$$

$$- \frac{1}{16}t_3(1+2x_3)(1+\alpha)\rho_0^{1+\alpha} - \frac{1}{8}t_4x_4(3\alpha_4+5)\left(\frac{3\pi^2}{2}\right)^{\frac{2}{3}}\rho_0^{\frac{5}{3}+\alpha_4} + \frac{1}{24}t_5(4+5x_5)(3\alpha_5+5)\left(\frac{3\pi^2}{2}\right)^{\frac{2}{3}}\rho_0^{\frac{5}{3}+\alpha_5}. \tag{24}$$

Moreover, the dimensionless Landau parameters F_0, F_1, F_0' are directly related to quantities describing nuclear matter such as effective mass, incompressibility, and symmetry energy through relationships

$$\frac{m^*}{m} = 1 + \frac{1}{3}F_1, \tag{25}$$

$$K = 3\frac{\hbar^2 k_F^2}{m^*}(1 + F_0), \tag{26}$$

$$E_{\rm sym} = \frac{\hbar^2 k_F^2}{6m^*}(1 + F_0'). \tag{27}$$

III. THE EXTENDED SKYRME INTERACTION PARAMETERS

Based on the procedure automatically searching for the standard Skyrme interaction parameters [9], we make a modification to optimize the extended Skyrme interaction parameters. It is well known that all properties of the nuclear matter are empirical quantities and derived from experiments indirectly in a model-dependent way, but they can offer an important insight into specific parts of the Skyrme interactions and have important applications in the nuclear theory, such as heavy-ion collisions and the neutron stars. In the present work, the properties of nuclear matter, the binding energies, charge rms radii of spherical even-even nuclei, and the properties of nuclear reaction are considered during automatical searching the extended Skyrme interaction parameters. For the properties of nuclear matter, the binding energy per nucleon E/A, the symmetry energy $E_{\rm sym}$, the incompressibility K, the effective nucleon mass m^*/m, and the equilibrium density ρ_0 are chosen. In the process of adjustment, these Skyrme parameters

are automatically performed to minimize a χ^2 quantity, which is written as

$$\chi^2 = \chi_{NR}^2 + \frac{1}{5}\sum_{i=1}^{5}\left(\frac{u_i^{th} - u_i^{em}}{\Delta u_i^{em}}\right)^2$$
$$+ \frac{1}{12}\sum_{i=1}^{12}\left[\left(\frac{E_{i,b}^{th} - E_{i,b}^{ex}}{\Delta E_{i,b}^{ex}}\right)^2 + \left(\frac{r_{i,ch}^{th} - r_{i,ch}^{ex}}{\Delta r_{i,ch}^{ex}}\right)^2\right], \tag{28}$$

where χ_{NR}^2 denote the χ^2 contributions of the total average nuclear reaction. u_i^{th} and u_i^{em} respectively represent the theoretical and empirical values for five controlled nuclear matter quantities. $E_{b,i}^{th}$, $E_{b,i}^{ex}$, $r_{ch,i}^{th}$, and $r_{ch,i}^{ex}$ represent the theoretical and experimental values for the binding energies and charge rms radii of 12 chosen spherical even-even nuclei, while Δu_i, $\Delta E_{b,i}$, and $\Delta r_{ch,i}$ denote the permissible values of these deviations.

For the properties of nuclear reaction, the total cross sections, nonelastic cross sections, elastic-scattering angular distributions, and analyzing powers are considered. We first obtain the χ^2 for each single target and then the average value of total χ^2 for all of targets are derived. The average value of total χ^2 is defined as

$$\chi_{NR}^2 = \frac{1}{N}\sum_{i=1}^{N}\left(\frac{\sigma_i^{th} - \sigma_i^{ex}}{\Delta\sigma_i^{ex}}\right)^2, \tag{29}$$

where N indicates the total number of experimental data in our consideration. σ_i^{th} and σ_i^{ex} are respectively the theoretically calculated value and the experimental value for the ith considered quantity. $\Delta\sigma$ is the experimental error of corresponding data.

TABLE I. The obtained extended Skyrme interaction parameters SkC17.

t_0 (MeV fm^3)	-1289.713
t_1 (MeV fm^5)	748.520
t_2 (MeV fm^5)	-77.489
t_3 (MeV fm$^{3+3\alpha}$)	12097.586
t_4 (MeV fm)	-1169.892
t_5 (MeV fm)	65.807
x_0	0.137
x_1	0.326
x_2	-0.0799
x_3	0.272
x_4	0.867
x_5	0.624
α	0.801
α_4	0.721
α_5	0.781
W_0 (MeV fm^5)	105.587

Furthermore, the experimental data of total cross sections, nonelastic cross sections, elastic-scattering angular distributions, and analyzing powers in the target mass range $24 \leqslant A \leqslant 209$ with incident neutron energies below 100 MeV are chosen in the fitting procedure. All of them are from the nuclear database EXFOR [24], which include those experimental data obtained from the global phenomenological optical potential, Koning-Delaroche (KD) potential [25], and some of the latest experimental data below 100 MeV. Since the nuclear reaction observables calculated with the extended Skyrme interaction GS2 [7] is the closest to the experimental data for all existing extended Skyrme interactions, we choose it as the original Skyrme interaction parameters. On the basis of the obtained MOP and the modified optimization procedure, we get a new set of extended Skyrme interaction parameters SkC17. The values of obtained extended Skyrme interaction parameters are listed in Table I.

IV. RESULTS AND DISCUSSION

A. Properties of finite nuclei

The nuclear ground-state properties can be calculated by the Skyrme-Hartree-Fock method, such as the binding energies, charge radii, single-particle energies, etc. The ground-state properties of finite nuclei are obtained by the new extended Skyrme interaction SkC17.

The relative deviations of the binding energies and charge rms radii calculated with the extended Skyrme interaction SkC17 from the corresponding experimental data [26,27] for 12 chosen spherical even-even nuclei are presented in Fig. 1. It can see that the results calculated with the extended Skyrme interaction SkC17 can well describe the binding energies and charge rms radii. The discrepancies relative to experimental data are within 1.5% for these nuclei and it is better than those results from the extended Skyrme interaction GS2 [7] and our standard Skyrme interaction SkC [9].

The extended Skyrme interaction SkC17 not only give a satisfactory description of the binding energies and charge rms
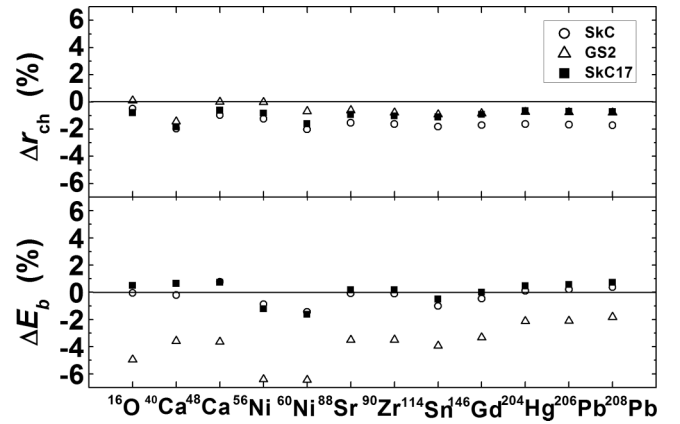

FIG. 1. Calculated the relative deviations of charge radii (upper panel) and energies per nucleon (lower panel) using SkC17, SkC, and GS2 for the selected nuclei.

radii but also reasonably predict the single-particle energies. The neutron and proton single-particle energy levels are predicted near the Fermi surface with the obtained Skyrme force SkC17 for ^{16}O, ^{40,48}Ca, ^{90}Zr, and ^{208}Pb. Figures 2 and 3 show the comparisons with the experimental data [2] and our standard Skyrme interactions SkC [9] for ^{208}Pb and are compared with those of extended Skyrme interactions BSk18 [15], eMSL07 [16], and SkOP4 [17], which are obtained by considering the spin-orbit splitting energy for neutron $3p_{1/2}$ and $3p_{3/2}$ levels for ^{208}Pb. As can be seen in these figures, the extended Skyrme interaction SkC17 describes the single-particle energies of the ^{208}Pb are generally not worse than the other extended Skyrme interactions obtained from fitting properties of finite nuclei and nuclear matter. Moreover, the SkC17 better describes the single-particle energies for ^{208}Pb comparing with the standard Skyrme interaction SkC.

B. Properties of nuclear matter

The main properties of the symmetric nuclear matter are calculated with the found extended Skyrme interaction SkC17, as well as the eight Landau parameters F_l, F_l', G_l, $F_l'(l = 0,1)$.
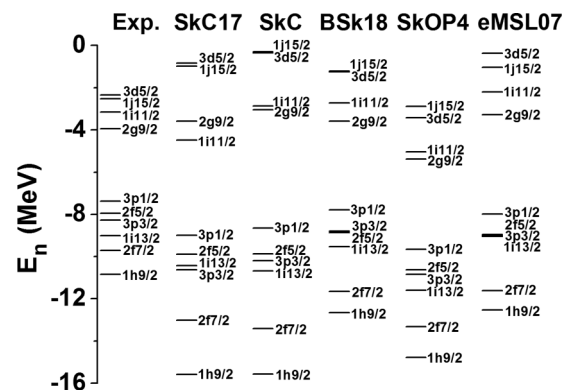

FIG. 2. Comparison of the neutron single-particle energy levels near the Fermi surface calculated using various Skyrme interactions with the experimental data [2] for ^{208}Pb.
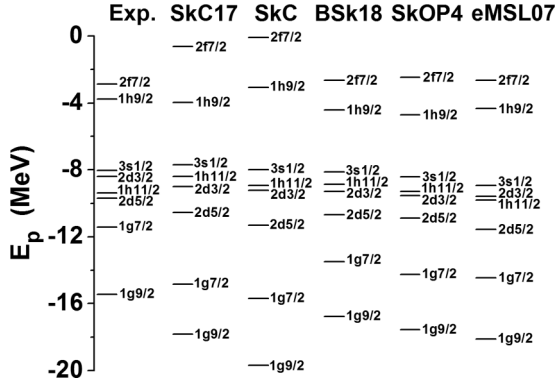
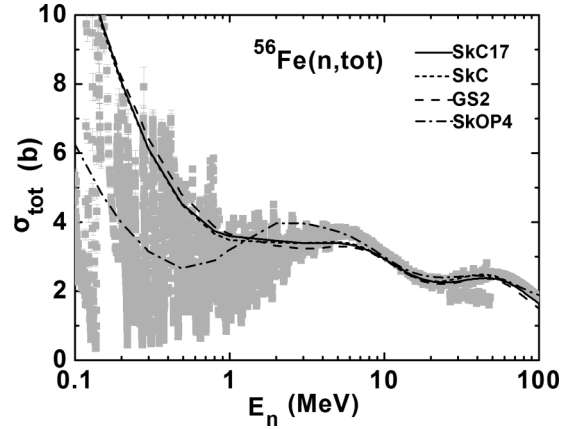FIG. 3. Same as Fig. 2, but of proton single-particle energy levels [2].

FIG. 4. Comparison of the total cross sections calculated using SkC17, SkC, GS2, and SkOP4 with experimental data (shaded area) [31,32] for ^{56}Fe.

The results are compared with those from SkC and other extended Skyrme interaction. The typical extended Skyrme parametrizations are chosen, such as GS2 [7], BSk18 [15], eMSL07 [16], and SkOP4 [17]. The comparisons are shown in Table II. It can see that the obtained equilibrium density ρ_0 and the energy per nucleon E/A both are very close to the empirical values ($\simeq 0.16$ fm^{-3} and $\simeq -16.0$ MeV). The incompressibility K and symmetry energy E_{sym} are also in the range of empirical quantities ($K = 230 \pm 30$ MeV and $27 < E_{\text{sym}} < 38$) [28]. The effective nucleon mass m^*/m has been established in which the m^* is lower than the m and is generally derived by fitting the experimental data of giant quadrupole resonance (GDR). There are four different cases in the current conclusion for m^*/m and they are respectively 0.6, 0.7, 0.8, and 0.9. However, the experimental GDR data on light and heavy nuclei cannot be satisfied simultaneously with the present form of the static HF functional and additional work is needed in both theory and experiment [28]. In particular, the density slope of symmetry energy $L(\rho_0)$ at saturation density is also predicted with the Skyrme interaction SkC17. It is in the recent constraint range from analysis of isospin diffusion and double neutron-proton ratio in heavy-ion collisions at intermediate energies, and requires $L = 58 \pm 18$ MeV [28–30]. For the

Landau parameters $F, F'(l = 0, 1)$, they are directly related to some nuclear matter properties [see Eqs. (25)–(27)] and demanded to be greater than $-(2l + 1)$. It can see that the obtained Landau parameters are reasonable.

C. The neutron scattering

In this section, the observables describing the neutron-induced reaction are calculated and compared with the corresponding experimental data. The total cross sections, nonelastic cross sections, elastic-scattering angular distributions, and analyzing powers for different targets with incident energies below 100 MeV are calculated. These results are also compared with those of standard Skyrme interaction SkC and the extended Skyrme interactions GS2 and SkOP4, which could give a better description of nuclear reaction properties than other existing extended interactions.

For the total cross sections, the narrow and broad resonances with large amplitudes appear for those light targets in the range of hundreds of keV to few MeV, where it just expected to provide smooth average results. The comparisons of total

TABLE II. The main nuclear-matter properties of different Skyrme interactions.

|	SkC17	SkC	GS2	BSk18	SkOP4	eMSL07
ρ_0 (fm^{-3})	0.159	0.162	0.159	0.159	0.159	0.158
E/A (MeV)	-16.08	-16.09	-16.02	-16.06	-16.02	-16.04
K (MeV)	258.16	285.02	300.19	241.83	222.67	229.77
m^*/m	0.66	0.56	0.60	0.80	0.75	0.70
E_{sym} (MeV)	29.61	30.81	25.96	30.00	30.87	32.71
$L(\rho_0)$	63.97	64.57	30.26	36.21	74.56	47.3
F_0	-0.19	-0.29	-0.18	-0.12	-0.24	-0.27
F_0'	0.73	0.38	0.27	0.97	0.90	0.88
F_1	-0.89	-1.33	-1.20	-0.60	-0.74	-0.90
F_1'	0.37	0.51	0.30	0.032	0.37	0.50
G_0	0.19	0.35	0.42	-0.33	-0.031	0.21
G_0'	0.42	0.30	0.35	0.46	0.45	0.24
G_1	0.54	0.44	0.73	1.23	0.61	0.22
G_1'	0.49	0.54	0.51	0.50	0.48	0.67
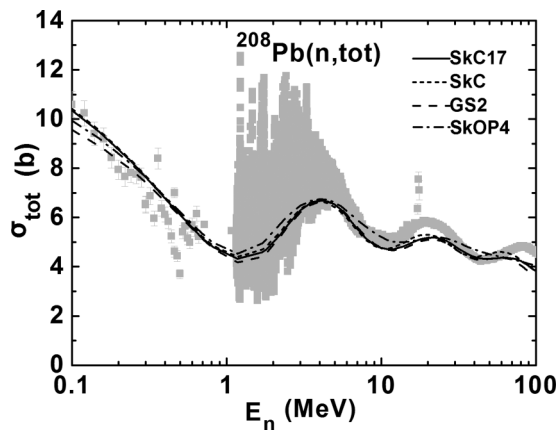
FIG. 5. Comparison of the total cross sections calculated using SkC17, SkC, GS2, and SkOP4 with experimental data (shaded area) [33–37] for ^{208}Pb.

cross sections calculated with the experimental data [31–37] for ^{56}Fe and ^{208}Pb are shown in Figs. 4 and 5. The usual agreement with the experimental data is obtained by the SkC17 and SkC for ^{56}Fe and the deviation of our calculations are within 7% on average. But the total cross sections calculated by the GS2 are smaller than the experimental data above 60 MeV. Moreover, the curve shape of total cross sections calculated by the SkOP4 are different from those of SkC17, SkC, GS2, and experimental data. For the heavy target ^{208}Pb, the total cross sections are underestimated by the SkC17, SkC, and SkOP4. The maximum deviation between experimental data and calculation is 15%, while the deviations with the GS2 are larger and as much as 22% above 65 MeV.

There are only the experimental data of nonelastic cross sections with incident neutron energies below 40 MeV for most targets. The latest experimental data [38], from 2002, are given for the natural nuclei ^{nat}Si, ^{nat}Fe, ^{nat}Zr, and ^{nat}Pb between 40 and 80 MeV. Figures 6 and 7 present the calculations of nonelastic cross sections for ^{56}Fe and ^{208}Pb. The results calculated with SkC17, SkC, and GS2 are consistent with experiment data in the error range [38–46] below 50 MeV.
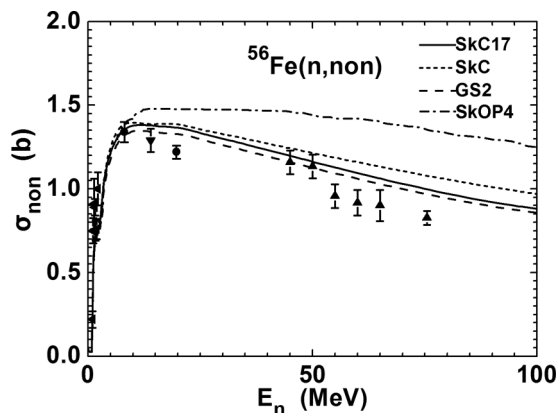

FIG. 6. Comparison of the nonelastic cross sections calculated using SkC17, SkC, GS2, and SkOP4 with experimental data (symbols) [38–41] for ^{56}Fe.
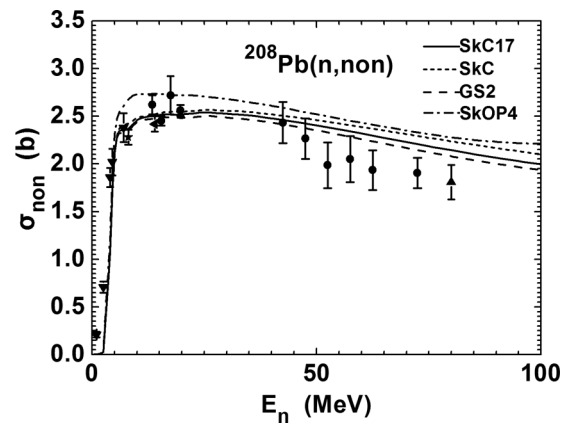

FIG. 7. Comparison of the nonelastic cross sections calculated using SkC17, SkC, GS2, and SkOP4 with experimental data (symbols) [38,40–46] for ^{208}Pb.

For higher energies, the results of nonelastic cross sections calculated with these Skyrme interactions are slightly larger than the experimental data, but the curve shapes are similar and the results of SkC17 and GS2 are closer to the experimental data than those of the standard Skyrme interaction SkC. The results calculated with SkOP4 are much larger than the experimental data and those of the other Skyrme interactions.

The elastic-scattering angular distributions are calculated by the SkC17 for different targets (from ^{24}Mg to ^{208}Pb) below
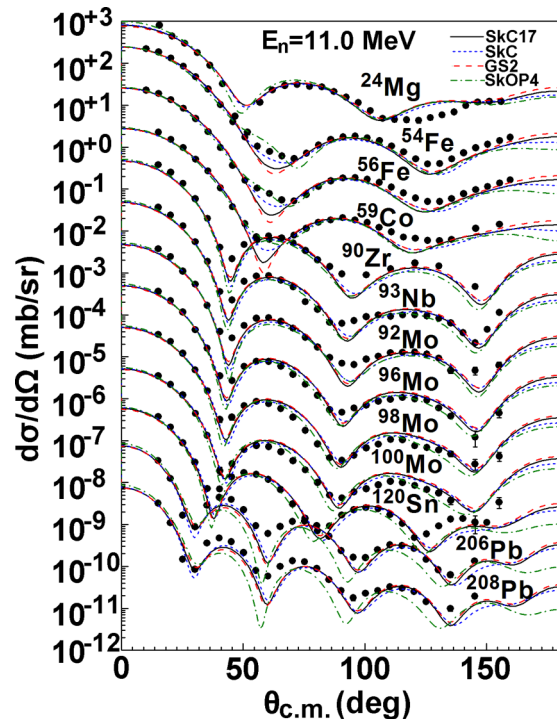

FIG. 8. Comparison of the elastic-scattering angular distributions with experimental data (symbols) [47–52] at incident neutron energies of 11.0 MeV. The results are respectively calculated by Skyrme interaction parameter SkC17, SkC, GS2, and SkOP4, which are offset by factors of 10.
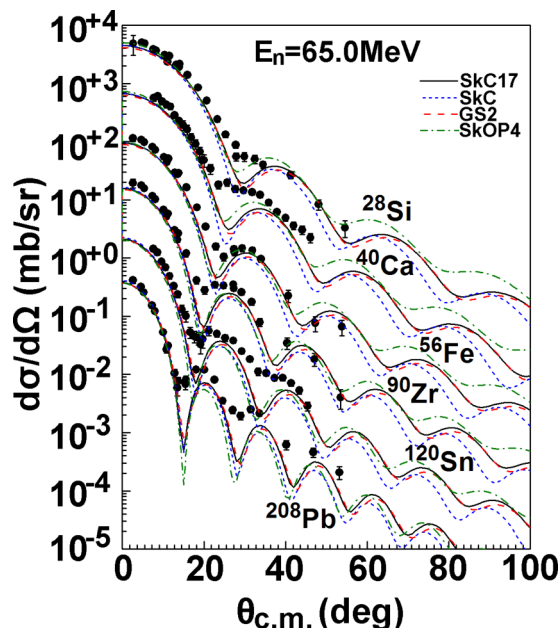
FIG. 9. Same as Fig. 8, but with incident energies 65.0 MeV [53,54].

100 MeV and then compared with those of standard Skyrme interaction SkC and the extended Skyrme interactions GS2 and SkOP4. These results of the Skyrme interactions SkC17, SkC, and GS2 are similar and show reasonable agreement with the experimental data for different targets below about 10 MeV. With the increasing incident energies, the results of the Skyrme interaction SkC17 are closer to the experimental data than those of the standard Skyrme interaction SkC, especially for the larger angles. For the Skyrme interaction SkOP4, the calculated elastic-scattering angular distributions are similar with those of the Skyrme interaction SkC17 for most of targets, while there are some discrepancies between them for some heavier nuclei. Figures 8 and 9 present the comparisons of the elastic-scattering angular distributions with experimental data [47–54] at incident energies of 11.0 and 65.0 MeV for different targets. In the following figures, the
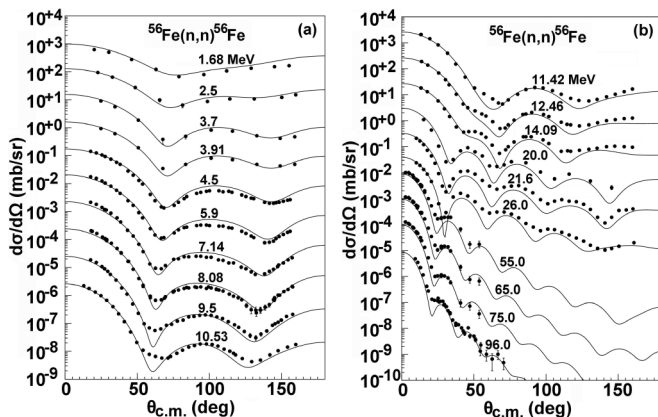

FIG. 10. Comparison of the elastic-scattering angular distributions calculated using SkC17 with experimental data (symbols) [47,55–60] for ^{56}Fe. The results are offset by factors of 10.
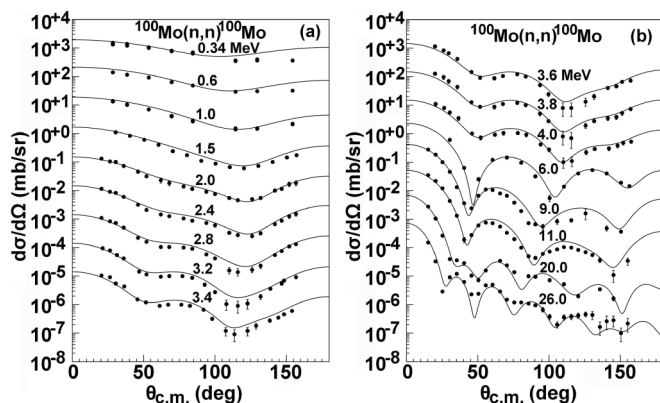

FIG. 11. Same as Fig. 10, but for ^{100}Mo [52,61–64].

calculations by the Skyrme interaction SkC17 are compared with the corresponding experimental data.

The elastic-scattering angular distributions for ^{56}Fe at incident energies from 1.68 to 96.0 MeV are given in Fig. 10. The calculated results are in good agreement with experimental data [47,55–60] except for the first minimum at 26.0 MeV, where the calculations give a slight underestimation of the experimental data. At the higher incident energies, the good agreements are present again. The elastic-scattering angular distributions for the isotopic chain ^{92,96,98,100}Mo are in good agreement with the corresponding experimental data below 26.0 MeV. The comparisons with the experimental data [52,61–64] for ^{100}Mo are given in Fig. 11.
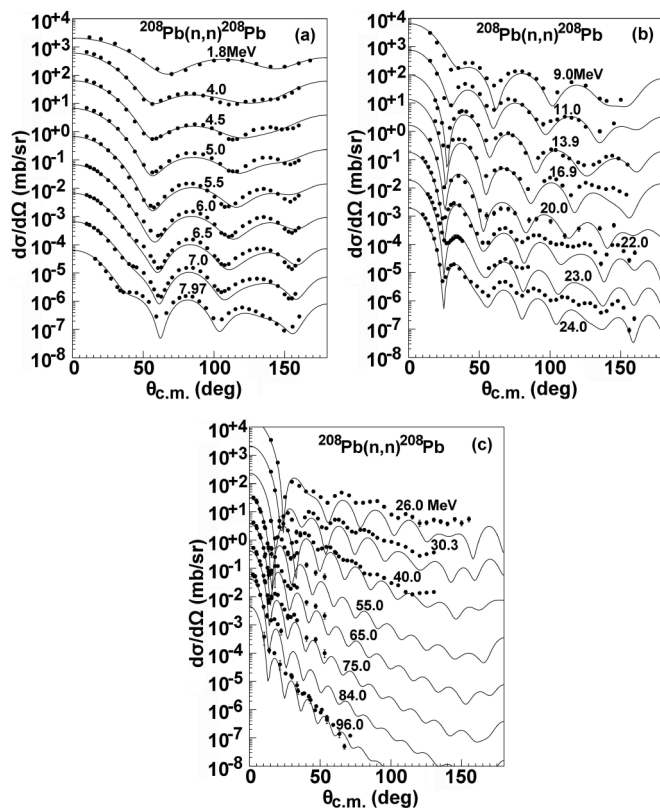

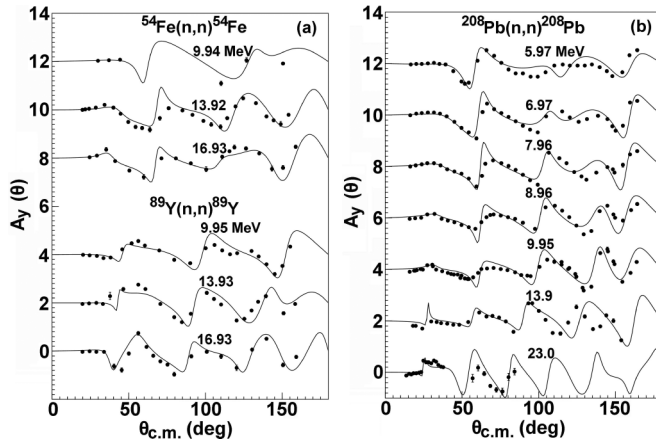FIG. 12. Same as Fig. 10, but for ^{208}Pb [51,55,65–72].

FIG. 13. Comparison of the analyzing powers calculated using SkC17 with experimental data (symbols) [67,69,70,73–75] for ^{54}Fe, ^{89}Y, and ^{208}Pb. The curves and data points at the bottom represent true values, while the others are added by 2.0.

Figure 12 shows the comparisons between the calculations and experimental data [51,55,65–72] for ^{208}Pb. The reasonable agreements are obtained below 13.9 MeV. There are a slight underestimation at other energies above 70 deg, but the curve shapes of present results and experimental data are similar.

As the achievement of the elastic-scattering angular distributions, we carry out the calculations of analyzing powers $A_y(\theta)$ for different targets and incident energies. The analyzing powers $A_y(\theta)$ for ^{54}Fe, ^{89}Y, and ^{208}Pb are plotted in Fig. 13. Obviously, the agreements of theoretical curves with experimental data [67,69,70,73–75] are also satisfactory.

The observables of nuclear reaction in the target mass range $12 \leqslant A \leqslant 24$ are further predicted at incident neutron energy below 100 MeV. Figure 14 gives the comparisons of elastic-scattering angular distributions predicted by the obtained extended Skyrem interaction SkC17 with the corresponding experimental data [53,72,76–87] for ^{12}C. The figure shows that satisfactory agreements are obtained between them. On the other hand, the observables of nuclear reaction for those
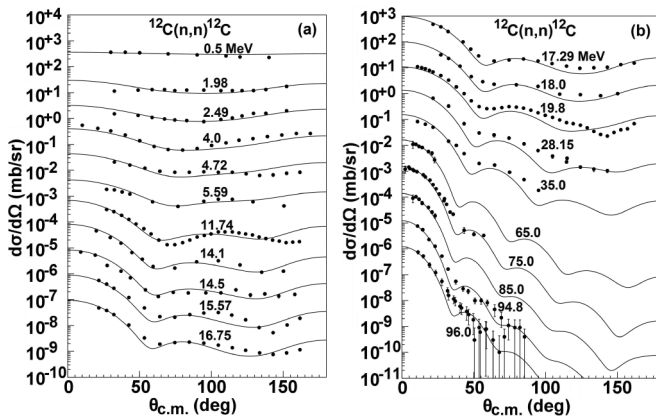

FIG. 14. Comparison of the elastic-scattering angular distributions predicted using SkC17 with experimental data (symbols) [53,72,76–87] for ^{12}C. The results are offset by factors of 10.
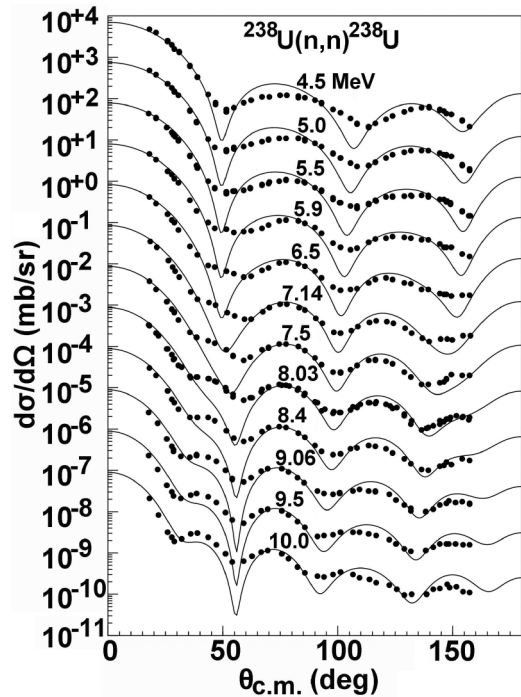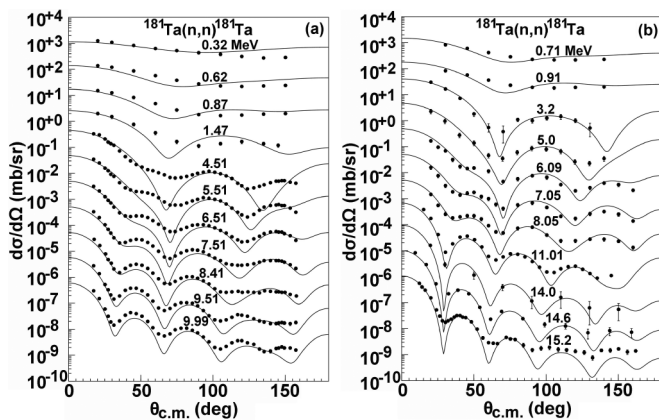

FIG. 15. Same as Fig. 14, but for ^{238}U [88].

targets in the mass range $209 < A \leqslant 239$, that is, actinide nuclei, are also predicted by the SkC17. In Fig. 15, the elastic-scattering angular distributions for ^{238}U are compared with the experimental data [88] and the largest deviations seem to occur for the first minimum. The reason is that the experimental data [88] include the elastic- and inelastic-scattering angular distributions, while our results are only the elastic-scattering results, and the coupling effect has been not considered between the elastic and inelastic scattering.

Furthermore, those nuclei in the mass range of $148 \leqslant A \leqslant 194$ have been widely investigated and there also have been some new experimental data in recent years. These superdeformed targets are rich in nuclear structure properties. The elastic-scattering angular distributions are also predicted by the found extended Skyrem interaction SkC17 for these targets below 100 MeV. Figure 16 shows the comparisons between the predicted elastic-scattering angular distributions and different experimental data for ^{181}Ta target. There are only experimental data below about 16 MeV and some experimental data of angular distributions include the results of elastic and inelastic scattering. In Fig. 16(a), it can be seen that the significant differences between the predicted results and the experimental data [89] appear near the first minimum, where the inelastic scattering is not included in the prediction. Figure 16(b) shows that the predicted results are in reasonable agreement with experimental data [50,90–95] except for incident energy 15.2 MeV above 100 deg, where they are slightly smaller than the experimental data including the inelastic scattering [95].

In this paper, we do not perform the calculations of proton elastic scattering, but the Coulomb potential of nucleus is considered in the MOP, so the description of proton-nucleus

FIG. 16. Same as Fig. 14, but for ^{181}Ta [50,89–95].

scattering with the found extended Skyrme interaction SkC17 is without any difficulties.

V. CONCLUSIONS

Within the framework of the extended Skyrme interaction involving the additional momentum- and density-dependent terms, we have found a new extended Skyrme interaction SkC17 by simultaneously fitting the experimental data of neutron-induced reaction below 100 MeV, including the total cross sections, reaction cross sections, elastic scattering angular distributions, and analyzing powers for the mass range $24 \leqslant A \leqslant 209$. During the fitting, we controlled the main properties of nuclear matter and finite nuclei. The newfound extended Skyrme interaction conforms to mostly recent constraints on main nuclear matter properties and provides a satisfactory description of the properties of ground state. The calculated results are further compared with those of conventional Skyrme interaction obtained in previous work of Ref. [9] and the existing extended Skyrme interactions. Comparisons show that the new extended Skyrme interaction improves the description of differential cross sections and analyzing powers of elastic scattering of neutron-induced various targets. Furthermore, the observable neutron-induced reactions predicted for light, actinide, and deformed nuclei give reasonable agreements with the corresponding experimental data. Therefore, the new extended Skyrme interaction obtained in the present work provides a unified approach to study the properties of nuclear matter, nuclear structure, nuclear reaction, and is appropriate for the prediction of unstable nuclear reaction.

[1] T. H. R. Skyrme, Philos. Mag. **1**, 1043 (1956).

[2] D. Vautherin and D. M. Brink, Phys. Rev. C **5**, 626 (1972).

[3] N. V. Giai and H. Sagawa, Phys. Lett. B **106**, 379 (1981).

[4] H. S. Kohler, Nucl. Phys. A **258**, 301 (1976).

[5] H. Krivine, J. Treiner, and O. Bohigas, Nucl. Phys. A **336**, 155 (1980).

[6] E. Chabanat, P. Bonche, P. Haensel, J. Meyer, and R. Schaeffer, Nucl. Phys. A **635**, 231 (1998).

[7] S. Krewald, V. Klemt, J. Speth, and A. Faessler, Nucl. Phys. A **281**, 166 (1977).

[8] V. V. Pilipenko, V. I. Kuprikov, and A. P. Soznik, Phys. Rev. C **81**, 044614 (2010).

[9] Y. L. Xu, H. R. Guo, Y. L. Han, and Q. B. Shen, J. Phys. G **41**, 015101 (2014).

[10] Y. L. Xu, Y. L. Han, and Q. B. Shen, Int. J. Mod. Phys. E **25**, 1650013 (2016).

[11] J. Margueron and H. Sagawa, J. Phys. G **36**, 125102 (2009).

[12] J. Margueron, S. Goriely, M. Grasso, G. Colo, and H. Sagawa, J. Phys. G **36**, 125103 (2009).

[13] N. Chamel and S. Goriely, Phys. Rev. C **82**, 045804 (2010).

[14] S. Goriely, N. Chamel, and J. M. Pearson, Phys. Rev. C **82**, 035804 (2010).

[15] N. Chamel, S. Goriely, and J. M. Pearson, Phys. Rev. C **80**, 065804 (2009).

[16] Z. Zhang and L.-W. Chen, Phys. Rev. C **94**, 064326 (2016).

[17] V. V. Pilipenko and V. I. Kuprikov, Phys. Rev. C **86**, 064613 (2012).

[18] Q. B. Shen, Y. L. Han, and H. R. Guo, Phys. Rev. C **80**, 024604 (2009).

[19] S. Goriely, N. Chamel, and J. M. Pearson, Phys. Rev. C **88**, 024308 (2013).

[20] J. W. Negele, Phys. Rev. C **1**, 1260 (1970).

[21] J. P. Jeukenne, A. Lejeune, and C. Mahaux, Phys. Rep. **25**, 83 (1976); Phys. Rev. C **16**, 80 (1977).

[22] Q. B. Shen, J. S. Zhang, Y. Tian, Z. Y. Ma, and Y. Z. Zhuo, Z. Phys. A **303**, 69 (1981); Commun. Theor. Phys. **2**, 1233 (1983).

[23] C. B. Dover and N. V. Giai, Nucl. Phys. A **190**, 373 (1972).

[24] http://www-nds.iaea.org/exfor/exfor.htm

[25] A. J. Koning and J. P. Delaroche, Nucl. Phys. A **713**, 231 (2003).

[26] I. Angeli, At. Data Nucl. Data Tables **87**, 185 (2004).

[27] R. B. Firestone, *Table of Isotopes*, 8th ed. (Wiley, New York, 1996).

[28] M. Dutra, O. Lourenco, J. S. Sa Martins, A. Delfino, J. R. Stone, and P. D. Stevenson, Phys. Rev. C **85**, 035201 (2012).

[29] B. A. Li, L. W. Chen, and C. M. Ko, Phys. Rep. **464**, 113 (2008).

[30] L. W. Chen, C. M. Ko, B. A. Li, and J. Xu, Phys. Rev. C **82**, 024321 (2010).

[31] F. G. Perey, T. A. Love, and W. E. Kinney, ORNL Report No. ORNL-4823, Oak Ridge National Laboratory, Oak Ridge, USA, 1972.

[32] W. P. Abfalterer, F. B. Bateman, F. S. Dietrich, R. W. Finlay, R. C. Haight, and G. L. Morgan, Phys. Rev. C **63**, 044608 (2001).

[33] R. W. Finlay, W. P. Abfalterer, G. Fink, E. Montei, T. Adami, P. W. Lisowski, G. L. Morgan, and R. C. Haight, Phys. Rev. C **47**, 237 (1993).

[34] D. G. Foster, Jr. and D. W. Glasgow, Phys. Rev. C **3**, 576 (1971).

[35] R. F. Carlton, R. R. Winters, J. A. Harvey, N. W. Hill, C. H. Johnson, and J. Schiedmayer, Bull. Am. Phys. Soc. **36**, 1349 (1991).

[36] M. Divadeenam, E. G. Bilpuch, and H. W. Newson, Dissertation Abstracts B (Sciences) **28**, 3834 (1968).

[37] V. V. Filippov and M. N. Nikolaev, Atomnaya Energiya **15**, 493 (1963).

[38] M. Ibaraki, M. Baba, T. Miura, T. Aoki, T. Hiroishi, H. Nakashima, S. Meigo, and S. Tanaka, J. Nucl. Sci. Technol. Suppl. **2**, 405 (2002).

[39] A. I. Abramov, Atomnaya Energiya **12**, 62 (1962).

[40] J. G. Degtjarev and V. G. Nadtochij, Atomnaya Energiya **11**, 397 (1961).

[41] J. G. Degtjarev, Atomnaya Energiya **19**, 456 (1965).

[42] J. R. Beyster, R. L. Henkel, R. A. Nobles, and J. M. Kister, Phys. Rev. **98**, 1216 (1955).

[43] J. R. Beyster, M. Walt, and E. W. Salmi, Phys. Rev. **104**, 1319 (1956).

[44] G. P. Millburn, W. Birnbaum, W. E. Crandall, and L. Schecte, Phys. Rev. **95**, 1268 (1954).

[45] B. Pal, A. Chatterjee, and A. M. Ghose, Nucl. Instrum. Methods **171**, 347 (1980).

[46] V. I. Strizhak, Atomnaya Energiya **2**, 68 (1957).

[47] S. Mellema, R. W. Finlay, F. S. Dietrich, and F. Petrovich, Phys. Rev. C **28**, 2267 (1983).

[48] D. E. Bainum, R. W. Finlay, J. Rapaport, M. H. Hadizadeh, and J. D. Carlson, Nucl. Phys. A **311**, 492 (1978).

[49] J. Rapaport, J. D. Carlson, D. Bainum, T. S. Cheema, and R. W. Finlay, Nucl. Phys. A **296**, 95 (1978).

[50] J. C. Ferrer, J. D. Carlson, and J. Rapaport, Nucl. Phys. A **275**, 325 (1977).

[51] J. Rapaport, M. Mirzaa, H. H. Hadizadeh, D. E. Bainum, and R. W. Finlay, Nucl. Phys. A **341**, 56 (1980).

[52] J. Rapaport, T. S. Cheema, D. E. Bainum, R. W. Finlay, and J. D. Carlson, Nucl. Phys. A **313**, 1 (1979).

[53] M. Ibaraki, M. Baba, T. Miura, Y. Hirasawa, Y. Nauchi, H. Nakashima, S.-i. Meigo, O. Iwamoto, and S. Tanaka, Nucl. Instrum. Methods Phys. Res., Sect. A **446**, 536 (2000).

[54] E. L. Hjort, F. P. Brady, J. L. Romero, J. R. Drummond, D. S. Sorenson, J. H. Osborne, B. McEachern, and L. F. Hansen, Phys. Rev. C **50**, 275 (1994).

[55] M. Ibaraki, M. Baba, T. Miura, Y. Nauchi, Y. Hirasawa, N. Hirakawa, H. Nakashima, S.-I. Meigo, O. Iwamoto, and S. Tanaka, J. Nucl. Sci. Technol. Suppl. **37**(Suppl. 1), 683 (2000).

[56] N. Olsson, B. Trostell, E. Ramstroem, and B. Holmqvist, Nucl. Phys. A **472**, 237 (1987).

[57] A. Ohrn, J. Blomgren, P. Andersson, A. Atac, C. Gustavsson, J. Klug, P. Mermod, S. Pomp, P. Wolniewicz, M. Osterlund *et al.*, Phys. Rev. C **77**, 024605 (2008).

[58] A. Smith and P. Guenther, Nucl. Sci. Eng. **73**, 186 (1980).

[59] A. Smith, Nucl. Phys. A **605**, 269 (1996).

[60] D. Schmidt, W. Mannhart, H. Klein, and R. Nolte, Rept: Phys. Techn. Bundesanst., Neutronenphysik Reports, No. 20, Braunschweig, Germany, 1994.

[61] F. D. McDaniel, J. D. Brandenberger, G. P. Glasgow, and H. G. Leighton, Phys. Rev. C **10**, 1087 (1974).

[62] P. Lambropoulos, P. Guenther, A. Smith, and J. Whalen, Nucl. Phys. A **201**, 1 (1973).

[63] A. B. Smith, P. Guenther, and J. Whalen, Nucl. Phys. A **244**, 213 (1975).

[64] F. D. McDaniel, J. D. Brandenberger, G. P. Glasgow, M. T. Mc ellistrem, and J. L. Weil, P, ERDA-NDC-9, 315, University of Kentucky, Lexington, USA, 1977.

[65] R. P. De Vito, Ph.D. thesis, Michigan State University, East Lansing, USA, 1980.

[66] A. Bratenahl, S. Fernbach, R. H. Hildebrand, C. E. Leith, and J. Moyer, Phys. Rev. **77**, 597 (1950).

[67] S. T. Lam, W. K. Dawson, S. A. Elbakr *et al.*, Phys. Rev. C **32**, 76 (1985).

[68] J. R. M. Annand, R. W. Finlay, and F. S. Dietrich, Nucl. Phys. A **443**, 249 (1985).

[69] M. L. Roberts, P. D. Felsher, G. J. Weisel, Z. Chen, C. R. Howell, W. Tornow, R. L. Walter, and D. J. Horen, Phys. Rev. C **44**, 2006 (1991).

[70] C. E. Floyd, Ph.D. thesis, Triangle Universities Nuclear Lab., Durham, USA, 1981.

[71] R. W. Finlay, J. R. M. Annand, T. S. Cheema, J. Rapaport, and F. S. Dietrich, Phys. Rev. C **30**, 796 (1984).

[72] J. Klug, J. Blomgren, A. Atac, B. Bergenwall *et al.*, Phys. Rev. C **68**, 064605 (2003).

[73] R. S. Pedroni, C. R. Howell, G. M. Honore, H. G. Pfutzner, R. C. Byrd, R. L. Walter, and J. P. Delaroche, Phys. Rev. C **38**, 2052 (1988).

[74] G. M. Honore, R. S. Pedroni, C. R. Howell, H. G. Pfutzner, R. C. Byrd, G. Tungate, and R. L. Walter, Phys. Rev. C **34**, 825 (1986).

[75] D. F. Coope, S. N. Tripathi, M. C. Schell, J. L. Weil, and M. T. McEllistrem, Phys. Rev. C **16**, 2223 (1977).

[76] P. Boschung, J. T. Lindow, and E. F. Shrader, Nucl. Phys. A **161**, 593 (1971).

[77] D. W. Glasgow, F. O. Purser, H. Hogue *et al.*, Nucl. Sci. Eng. **61**, 521 (1976).

[78] Z. M. Chen, K. Baird, C. R. Howell, M. L. Roberts, W. Tornow, and R. L. Walter, J. Phys. G **19**, 877 (1991).

[79] J. H. Osborne, F. P. Brady, J. L. Romero *et al.*, Phys. Rev. C **70**, 054613 (2004).

[80] E. Arai (private communication).

[81] F. Demanins, L. Granata, G. Nardelli, G. Pauli, U. Abbondanno, F. Demanins, M. Lagonegro, and G. Nardelli, Report: INFN Reports, No. 73, University Trieste, Trieste, Italy, 1973.

[82] U. Fasoli, A. Metellini, D. Toniolo, and G. Zago, Nucl. Phys. A **205**, 305 (1973).

[83] N. Olsson, B. Trostell, and E. Ramstroem, Phys. Med. Biol. **34**, 909 (1988).

[84] Y. Yamanouti, M. Sugimoto, S. Chiba, M. Mizumoto, Y. Watanabe, and K. Hasegawa, Report: JAERI-M Reports, No. 89, Japan Atomic Energy Agency (JAEA), Ibaraki, Japan, 1989.

[85] T. Niizeki, H. Orihara, K. Ishii, K. Maeda, M. Kabasawa, Y. Takahashi, and K. Miuba, Nucl. Instrum. Methods Phys. Res., Sect. A **287**, 455 (1990).

[86] P. Mermod, J. Blomgren, C. Johansson *et al.*, Phys. Rev. C **74**, 054002 (2006).

[87] M. Baba, S. Matsuyama, M. Ishikawa, S. Chiba, T. Sakase, and N. Hirakawa, Nucl. Instrum. Methods Phys. Res., Sect. A **366**, 354 (1995).

[88] A. Smith and S. Chiba, Ann. Nucl. Energy **23**, 459 (1996).

[89] A. B. Smith, Report: ANL-NDM, No. 160, Argonne National Laboratory, Argonne, USA, 2005.

[90] R. L. Becker, W. G. Guindon, and G. J. Smith, Nucl. Phys. **89**, 154 (1966).

[91] L. F. Hansen, F. S. Dietrich, B. A. Pohl, C. H. Poppe, and C. Wong, Phys. Rev. C **31**, 111 (1985).

[92] L. Rosen and L. Stewart, Phys. Rev. **107**, 824 (1957).

[93] S. C. Buccino, C. E. Hollandsworth, and P. R. Bevington, Z. Phys. **196**, 103 (1966).

[94] B. Holmqvist, T. Wiedling, S. G. Johansson, G. Lodin, A. Kiss, B. Gustavsson, and B. Antolkovic, Report: Aktiebolaget Atomenergi, Stockholm/Studsvik, No. 366, Sweden, 1969.

[95] C. I. Hudson, Jr., W. S. Walker, and S. Berko, Phys. Rev. **128**, 1271 (1962).